Measurement of submicrometer diameters of tapered optical fibres using scanning electron microscopy

von
Dimitri Pritzkau

Diplomarbeit in Physik

angefertigt am
Institut für Angewandte Physik

vorgelegt der
Mathematisch-Naturwissenschaftlichen Fakultät
der Rheinischen Friedrich-Wilhelms-Universität
Bonn
im März 2010

Referent: Prof. Dr. D. Meschede
Korreferent: Prof. Dr. M. Weitz

Contents

1. Introduction

Since the idea of a scanning particle beam was proposed in 1929 [1], the scanning electron microscopy (SEM) attracted much interest. It gave the opportunity to enter the completely new field of submicrometre microscopy. However, the first electron microscope, developed in 1932 [2], could not reach the submicrimetre resolution. After the WWII the development of the electron microscopy was enhanced by the technological progress. In the present days resolution of several nanometers are achievable.

The electron microscopy boosts the research in biology, microbiology and material science. Most people, who have seen SEM images, remember nice pictures of insects, bacteria or viruses but only a small amount of them knows that the electron microscopy can provide more than just a nice picture.

In modern nanoparticle and semiconductor science the SEM is used to measure sizes of particles or the roughness of surfaces. Lets put it this way, the electron microscope is used as an oversized and overpriced ruler for quite small particles. Although the modern electron microscopes provide high resolution, achieving high accuracy can be very challenging. The following question have to answered first:

- How do the electrons interact with the specimen?

- Where does the specimen response signal come from?

- How does the specimen influence the measurement and on the other hand, how does the electron beam influence the specimen?

- Which model can be used to detect the specimen edges?

- How to obtain high resolution?

During my work I have answered these question by designing a diameter measurement technique for submicrometre diameter optical fibres with a scanning electron microscope. My task was to prepare the tapered fibre for SEM measurement, to operate the electron microscope and to analyse the data. The obtained diameter was used to verify an optical diameter measurement technique, which our group has developed.

2. Tapered optical fibre

In the past years, tapered optical fibres arouse great interest in different fields of optics and laser physics [3, 4]. This chapter gives a short introduction into the properties and applications of tapered optical fibres. Furthermore the importance of knowing the fibre diameter very precisely is mentioned.

Our group has developed a non destructive optical diameter measurement technique which is shortly described. The new technique requires a verification method. In the last part of the chapter the available verification techniques are described and compared to choose the most suitable method.

2.1. Submicrometre optical fibre

Tapered optical fibres are produced from standard single mode silica fibres with a cladding diameter of 125 µm and a core diameter of about 5 µm. The tapered region is manufactured by the flame-brushing technique [5, 6], which means that the standard fibre is heated up and pulled so that the diameter of the heated part can be decreased down to 100 nm. While pulling, the flame is moved along the fibre to provide a homogeneous waist with a length between 1 and 50 mm.
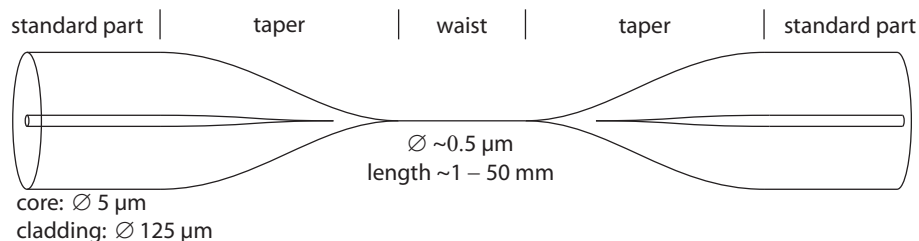

Figure 2.1.: Shape of a tapered optical fibre.

Light, propagating through the standard part, is weekly guided by the core-cladding interface. Therefore most of the intensity is located in the core. In the fibre waist, the light is strongly guided by the silica-air interface. Since the waist diameter is on the order of the light wavelength, an evanescent field appears in the fibre waist. The confinement of the light in the submicrometre fibre results in high intensity.

High light intensity, evanescent field and long interaction region are used in different applications such as supercontinuum generation [7], evanescent wave

spectroscopy of atoms [8] and molecules [9], nonlinear light-matter interaction in quantum optics [10]. Knowing the waist diameter precisely is critical for quantitatively understanding and controlling light propagation and nonlinear effects in tapered optical fibres.

2.2. Fibre diameter measurement using harmonic generation

The computer controlled pulling machine produces tapered fibres with the diameter precision of 5 %, which was exemplary checked for several samples with a scanning electron microscope [6]. Sinse the scanning electron measurement is distructive, the diameter of a newly produced fibre can not be checked with this method. Thus, a nondestructive optical diameter measurement technique is required. F. Warken used a diffractive tecnhnique by illuminating the fibre from the side and analysing the diffracted light. An accuracy of 50 nm for a fibre diameter of 1.32 µm was achieved [11]. An other method [12] measures the uniformity of the fibre diameter with a precision of $2 - 3$ % without giving an information about the diameter.

We developed a diameter measurement technique, based on second[1]- and third-harmonic generation in submicrometre diameter tapered fibres that provides an accuracy better than 2 % [17]. It takes the advantage of accomplishing phase matching between the fundamental and the harmonic light. The phase matching is realised when the phase velocities ν_{ph} of the fundamental and the harmonic waves are equal. The phase velocity depends on the effective refractive index n_{eff}, $\nu_{\mathrm{ph}} = c/n_{\mathrm{eff}}$ [18, chap. 12], which leads to the phase matching condition

$$n_{\mathrm{eff}}(\mathrm{fund}) = n_{\mathrm{eff}}(\mathrm{harm}), \qquad (2.1)$$

where $n_{\mathrm{eff}}(\mathrm{fund})$ ($n_{\mathrm{eff}}(\mathrm{harm})$) is the effective refractive index of the fundamental (harmonic) wave.

The n_{eff} can be calculated by numerically solving the eigenvalue equation for a step-fibre [18, 19] taking into account the material dispersion and the strong guidance of subwavelength-diameter fibre. Fig. 2.2a shows n_{eff} depending on the fibre diameter for the fundamental wave in the lowest order mode (HE_{11}) and three higher modes (TE_{01}, TM_{01}, HE_{21}) of the second-harmonic wave. The three intersections are the phase matching points.

When the wavelength is changed the intersection points occur at an other diameter (Fig. 2.2b). Thus, the Phase matching condition gives a one to one

---

[1]Second harmonic generation in centrosymmetric media was already observed [13, 14] and studied [15, 16].

relationship between the fibre diameter and the phase-matching wavelength. Therefore we can deduce the diameter of the fibre waist from the harmonic
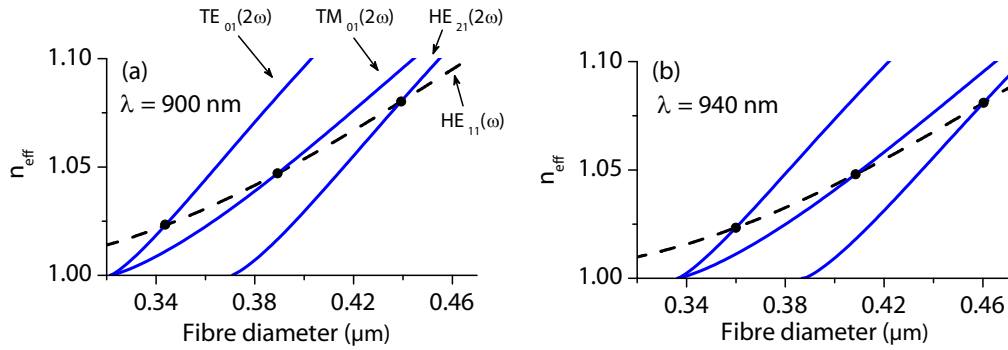

Figure 2.2.: Effective refractive index for the fundamental wave (dashed line) and corresponding second harmonic wave (continuous lines) depending on the diameter of the fibre. The phase matching condition (2.1) is fulfilled at the intersection points.

spectrum.

Fig. 2.3 illustrates the relationship between the fibre diameter and the phase-matching wavelength showing the second-harmonic spectrum and the converted diameter scale. The spectrum can be interpreted as the frequency of occurrence of a diameter. Thus, the main peak is equivalent to the dominating diameter whereas the leftmost peak corresponds to smaller diameter. On the left side the spectrum shows a cut-off indicating the absence of smaller diameters. The right tail of the spectrum occurs at higher diameter, thus it can be attributed to the fibre taper.

The value of the dominating diameter as well as the interpretation of the spectrum have to validated. The appropriate verification techniques are compared in the following section.

2.3. Verification technique

To verify the optical method a fibre diameter measurement technique is needed that provides an accuracy similar to our measurement technique of $< \pm 2$ %. Additionally, the verification technique should enable measuring the whole fibre waist (5 cm long) to obtain information about the diameter homogeneity to interpret the harmonic spectrum.

The following measurement methods are compared to choose the most appropriate technique.
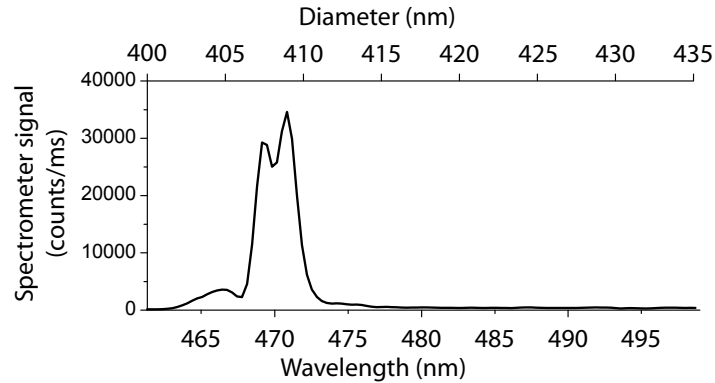
Figure 2.3.: Second harmonic response spectrum of a submicrometre diameter tapered optical fibre.

- Diffraction technique

- (Scanning) Transmission electron microscopy (TEM, STEM)

- Scanning electron microscopy (SEM)

The diffraction method (Sec. 2.2), is not suitable for verification of our method providing an accuracy of about ± 50 nm, .

The TEM is a technique whereby an ultra thin specimen is exposed by a collimated electron beam. The transmitted electrons form a diffraction pattern which is detected on an imaging device. The TEM can be operated in the STEM mode which means that the specimen is scanned with a focussed electron beam. The accuracy of both techniques is $\sim \pm 10$ nm for a 400 nm fibre (estimated, was not further investigated). The standard TEM (STEM) sample holder limits the fibre length to 2 mm, which makes impossible to measure the whole fibre waist.

The SEM uses a focussed electron beam to scan the specimen in a raster scan pattern (similar to STEM). Electrons interacting with the specimen atoms create a reflected response signal containing information about the sample surface topology. The accuracy of a scanning electron microscope is $\sim \pm 20$ nm for a fibre of 400 nm in diameter. The maximum sample size for a SEM is 10×10 cm, which enables measuring the whole fibre waist and the tapers.

The accuracy of the TEM as well as the SEM can be improved by recalibrating the microscope and using an appropriate model for fibre edge determination. SEM additionally allows to measure the whole waist and the tapers, which can give the information about the homogeneity of the fibre waist.

We decided to use the scanning electron microscope, which was kindly provided by the Center of Advanced European Studies and Research (CAESAR). My task was to

1. improve the accuracy of the microscope

2. develop a fibre preparation technique for SEM

3. design an imaging procedure

4. do the image analysis.

In the following I illustrate how I accomplished the task to verify the harmonic-generation diameter measurement technique.

3. Scanning electron microscope

The Center of Advanced European Studies and Research (CAESAR) provided me with access to the Zeiss SUPRA 55 equipped with the Gemini objective. In order to obtain high accuracy I had to determine the measurement parameters. Therefore the understanding of the setup and the operating principle of the scanning electron microscope are required.

3.1. Supra 55

The Supra 55 with Gemini objective is a field-emission SEM (FESEM). As an electron source it uses a field emission gun [20] that yields a spectrally narrow electron beam. The objective accelerates the beam to an energy between 1 and 30 keV, and focusses the beam on the specimen surface using magnetic and electrostatic lenses (Fig. 3.1). The lenses cause aberrations of two main types.
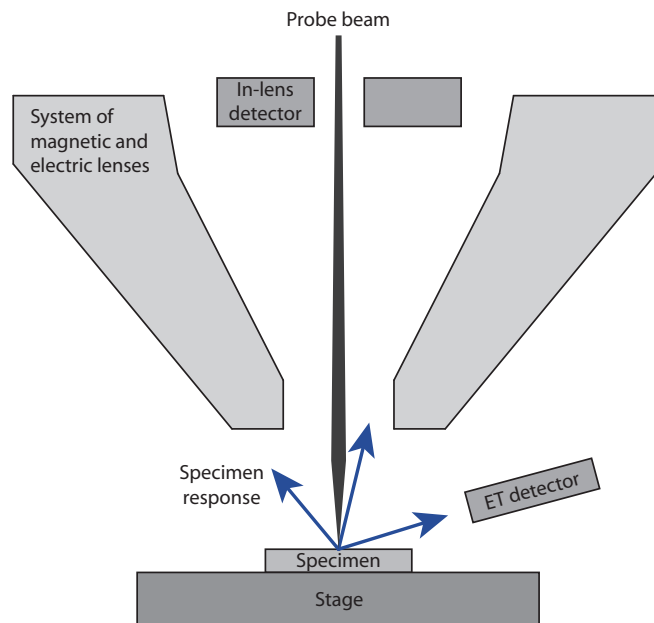

Figure 3.1.: Setup of the Supra 55.

The first one, the astigmatism, is the ellipticity of the electron beam. The

second one is the deviation of the beam from the surface normal. Stigmator and apertures should be adjusted to minimise aberrations before taking images. All types of aberrations and their influence on the imaging are described in [21, page 48].

Furthermore the objective realises the scanning procedure by moving the beam transversally to the specimen surface. The electron response signal is detected and saved separately for each position of the beam. This gives a two dimensional array of intensity values that is saved in a grey-scale image (typically 1024×768 pixels). Therefore the scanned region is equivalent to the field of view of the SEM image. SUPRA 55 provides a magnification up to $900\,000$ times and a scanning speed ranging from 30 ms/frame to 20 min/frame.

The response signal intensity can be measured by two different detectors: the Everhart-Thorney detector (ET detector) and the in-lens detector. The ET detector [22] is positioned sidewards of the specimen whereas the in-lens detector is built as a ring around the electron probe beam inside the objective (Fig. 3.1). The ET detector is used for general purposes [23], e.i. the entire probe energy range of 1–30 keV, high and low magnifications. The in-lens detector is limited to the beam energy range of 1–20 keV and used at high magnification. The in-lens detector is more sensitive to slopes and edges on the sample surface [23]. Therefore we use this detector for fibre imaging.

The specimen response signal depends on the following microscope settings

- Probe beam energy

- Probe beam current

- Magnification

- Scanning speed

- Distance between the stage and the objective

In order to determine the settings, the understanding of the electron-specimen interaction is needed.

3.2. Electron-specimen interaction

The probe electrons (PE), penetrating the specimen interact with the specimen atoms in two different ways. On the one hand, the probe electrons are elastically scattered on the atomic nuclei. On the other hand, the probe electrons scatter inelastically on the atoms. Each probe electron experiences both types of scattering during propagation through the specimen.
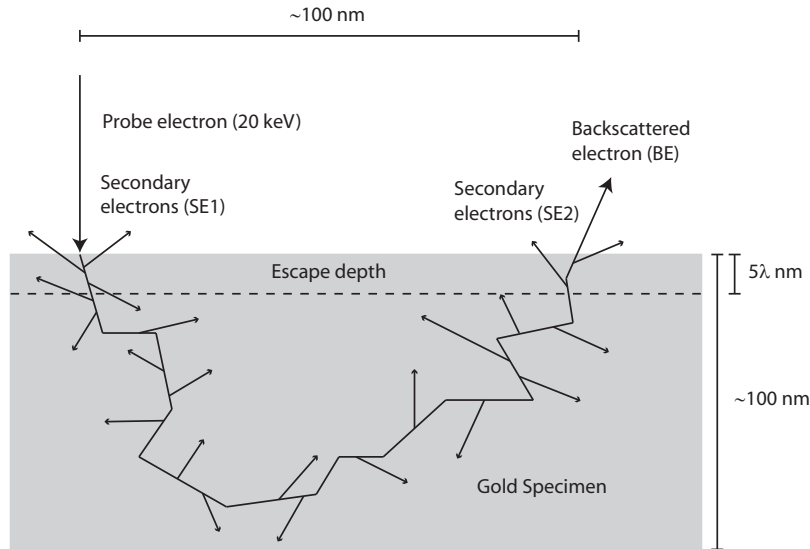
Figure 3.2.: Electron-specimen interaction. Probe electron scatters elastically and inelastically before escaping the specimen as a backscattered electron. Inelastic scattering generates secondary electrons. The maximal escape depth of the secondary electrons is 5λ [29]. SE1, SE2 and BE form the total specimen response.

Elastic scattering can be described by Rutherford scattering [24]. It changes significantly the propagation direction of the probe electron while almost maintaining the kinetic energy [21, p. 75]. Due to the high change in propagation direction, some probe electrons can escape the specimen (backscattered electrons, BE) and be detected (Fig. 3.2). The BE energy is typically a few percent smaller than the PE energy.

Unlike elastic scattering, the inelastic scattering causes a higher energy and a lower change in the propagation direction of the probe electrons. This mechanism can be described by the Bethe equation [25]. During inelastic scattering loosely bound electrons are excited (secondary electrons, SE). The energy transfer to each secondary electron is less than 50 eV [26, 27]. Thus the kinetic energy of a secondary electron is considerably smaller than the kinetic energy of a probe electron [28].

All along their trajectory in the specimen, probe electrons create secondary electrons, which then propagate through the specimen (Fig. 3.2). Some of them can escape the specimen and be detected. The probability p_{esc} for a secondary electron to escape the specimen depends on the depth z at which it is created

[27]:

$$p_{esc} \propto \exp(-\frac{z}{\lambda}) \tag{3.1}$$

where λ is the mean free path of the secondary electron. Generally, the maximum escape depth is considered to be 5λ [29]. For metals, λ is ~ 1 nm, whereas for insulators $\lambda \sim 10$ nm.

Therefore the secondary electrons can be split into two types: secondary electrons generated close to the probe beam (SE1), and those generated close to the escape point of a backscattered electron (SE2) (Fig. 3.2). Therefore the SE1 spacial distribution corresponds to the probe beam intensity distribution, whereas the SE2 and BE distributions are equally shaped (Fig. 3.3).
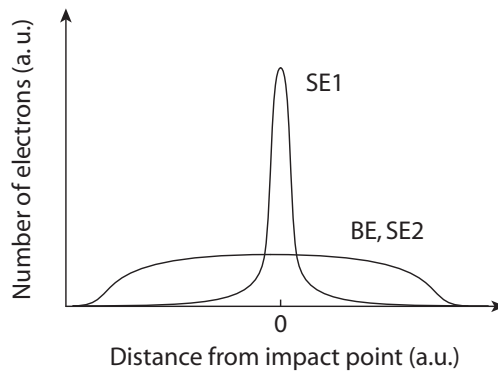

Figure 3.3.: Spacial distribution BE, SE2 and SE1 signals on the specimen surface

The SE2 signal provides a high resolution related to the probe beam diameter, which is ~ 2 nm (according to Zeiss). The BE and SE2 signals distribution, however, depends on the probe beam energy and the sample material. Therefore the appropriate probe beam energy has to be chosen to achieve the highest possible resolution.

3.3. Achieving high resolution

The probe beam energy influences the spacial distribution of the BE and the SE2 signals. Tab. 3.1 shows the spacial width for the energy limits our SUPRA 55 provides. Although the BE, SE2 spacial distribution width ranges from 10 to 2000 nm (Tab. 3.1), a high resolution can be obtained by choosing the appropriate ratio between the field of view and the width of the BE distribution. A spacial distribution, bigger than the field of view, results in a constant background signal that does not influence the resolution.

Probe electron energy	Spacial width	
	SE1	BE, SE2
1 keV	2 nm	10 nm
20 keV	2 nm	2000 nm

Table 3.1.: Estimation of the spacial width of the SE1, BE and SE2 signals in a gold specimen. Simulated with Casino software [30].

Since the measured fibre is typically less than one micrometre in diameter, the field of view is smaller than $1\,\mu m \times 1\,\mu m$ (magnification of $\sim 500\,000$). Therefore the PE energy of 20 keV gives the appropriate resolution.

3.4. Fibre damage by probe beam

The focussed probe beam, scanning over the fibre, can decrease its diameter. Fig. 3.4 illustrates a fibre section that was narrowed by the probe beam exposure. The narrowed part appeared while scanning the fibre with a magnification
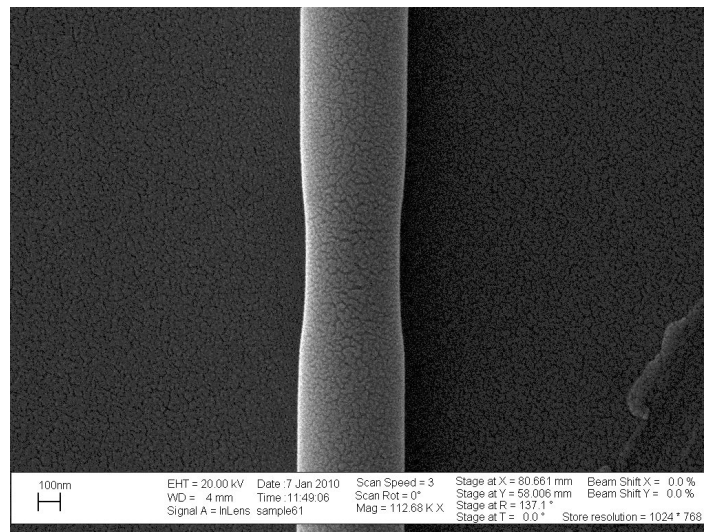

Figure 3.4.: A fibre section which was narrowed by probe beam exposure. The structure on the surface is due to gold coating (Sec. 4.2).

of about $500\,000$ times for several seconds. After that the magnification was decreased to circa $100\,000$ times and the image 3.4 was saved.

When scanning started, the fibre diameter started to decrease rapidly. Af-

17

ter some time (tens of seconds), the narrowing slowed down. This effect was stronger for higher beam currents and higher magnifications. The most probable explanation for the diameter decrease is the heating due to probe beam and pulling due to tension in the fibre. Since the fibre is an insulator, it could reach temperatures up to 1700 °C depending on the beam current [31, p. 65]. The tension could come from mounting the fibre on the gold wafer (section 4.1). It could be so strong, that a fibre could even break. Fig. C.2 shows such a sample.

to prevent narrowing the probe bean had to be minimized. It could be adjusted by setting the smallest aperture diaphragm in the microscope objective, but it could not be measured while imaging. The easiest way to get a value proportional to the beam current was to measure the current between the specimen and the ground (specimen current). The specimen current is a sum of the beam current and the SE current, which depends on the beam energy. The SE current can be both higher or lower than the probe current, so the specimen current of two measurements can only be compared for the same probe energy. For the fibre diameter measurement, I use the smallest aperture (7.5 µm) and hence the lowest specimen current (typically 20 pA).

The low signal-to-noise ratio, resulting from the low current, had to be compensated by a high integration time, hence low scanning speed. A low scanning speed led to long exposure time, which increases heating of the fibre. I decide to take images at two different scan speeds – 300 ms/frame and 2.4 s/frame – to be able to consider the influence of the scan speed on the diameter measurement.

3.5. Increasing detection efficiency

The signal-to-noise ratio can be further increased by improving the detecting efficiency of the secondary electrons. This is done by setting the specimen-objective distance (working distance) to 4 mm. The small distance allowed the magnetic field of the lens to reach the specimen. Since the SE energy was lower than 50 eV (Sec. 3.2) the secondary electrons were effected by the magnetic field and guided into the objective where they could be detected. In this way the detection efficiency of the SE signal was increased. The fast backscattered electrons are effected by the magnetic field only a little, and are not directed to the detector (see Fig. 3.5).

Probe beam

Magnetic lens

Detector

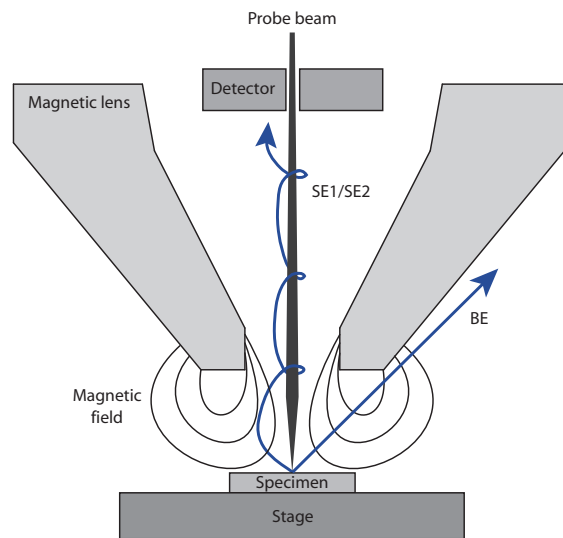SE1/SE2

BE

Magnetic
field

Specimen

Stage

Figure 3.5.: Magnetic field, created by the lens, guides the secondary electrons into the lens where they are detected. The fast backscattered electrons are almost not effected by the magnetic field.

4. Fibre preparation

The fibre was originally placed in a holder used for optical measurements. Inside the holder it was glued at two points to the holder, so the waist was hanging between these two points. For SEM imaging this design led to undesired vibration of the fibre waist. The electron bombardment additionally charged the fibre, since silica is an insulator. To prevent vibration and charging, I fixed the fibre waist on a substrate with a flat and conductive surface. Although the substrate provided excellent conductivity, the fibre still could be charged (Fig. C.1). Therefore I used additional metal coating after fixing the fibre to the gold wafer.

4.1. Fixing the fibre

To fix the fibre waist on the substrate, I used a home made insert for the optical holder. The insert is schematically illustrated in Fig. 4.1. The substrate(Fig. 4.1) was cut from a gold coated silicon wafer which was produced at CAESAR as a 4 inch disc. Between the gold and the silicon a chromium layer acted as an adhesive. The substrate was glued to the insert using conductive glue (Fig. 4.1). I positioned the insert below the optical holder (Fig. 4.2a) and moved the holder carefully down using translation stages. From above, the reflection of the fibre on the gold layer could be seen. When the fibre coincided with the reflection, it touched the substrate and I stopped moving the stages. If the fibre was well positioned on the substrate (Fig. 4.3a), I screw the insert to the holder.
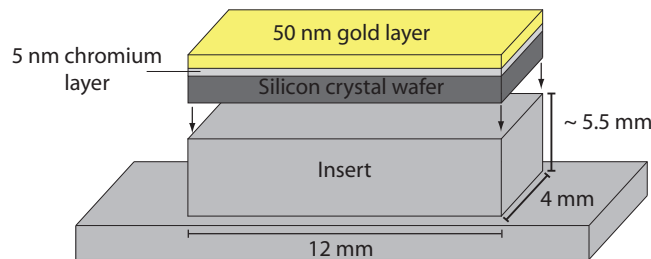

Figure 4.1.: Gold coated wafer over the insert. The wafer is glued to the insert by silver paint

Some fibres did not lie on the substrate in a proper way (Fig. 4.3b). The fibre waist could be tilted relatively to the substrate or shifted to one side. The tilt

was probably due to clamping of the fibre in the pulling machine. To prevent the tilting, each fibre could be checked with the optical microscope built into the pulling machine. The most probable reason for the shift was the initial position of the stages in the pulling machine. Nevertheless, I could fix such fibres on the substrate by tilting the insert and shifting the substrate in the direction of the waist.

When the fibre waist lied on the gold wafer, I applied one drop of conductive glue on each side of the substrate to prevent the fibre waist from being stripped of the substrate during the coating process (Sec. 4.2).
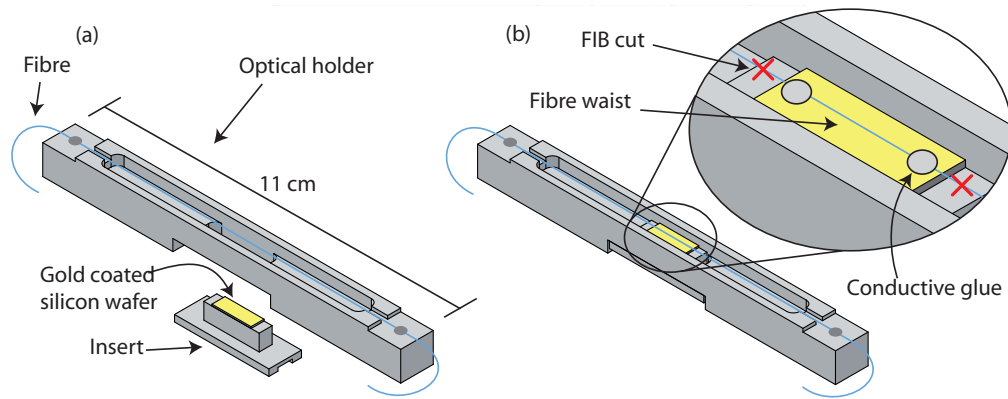
Figure 4.2.: (a) Tapered fibre in the optical fibre holder. The aluminium insert is placed below the holder. The substrate is glued on the insert. (b) Insert placed into the holder. Zoom on the wafer: fibre waist fixed with conductive glue on the substrate, outside the substrate the fibre is cut by focused ion beam (FIB)

In order to remove the insert from the holder, the fibre had to be cut outside of the substrate (Fig. 4.2b). The cutting was done by a focused ion beam (FIB) at CAESAR.

(a) Well positioned   **(b)** Badly positioned

Figure 4.3.: Position of the fibre relatively to the insert.

The FIB apparatus was integrated into another SEM, so I could see whether

the fibre contacted the substrate everywhere along the waist or it hung a few micrometres above it. If the fibre waist was hanging above the substrate we cut it on the inner side of the silver drops using the FIB to ensure continuous contact between the fibre and the substrate. After removing the fib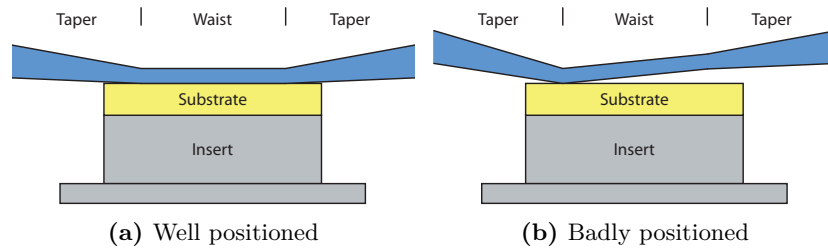re sample from the FIB, I applied additional glue drops on the ends of the substrate. At this point the fibre was ready to be coated.

4.2. Coating

A metal coating was used to prevent the fibre from being charged. The commercially available and commonly used techniques are the sputtering and the evaporating procedure. Echlin describes in his book [32] in details the application possibilities as well as the advantages and the disadvantages.

I used the Bal-Tec MED 020 sputtering machine that was available at CAESAR. This machine performed sputtering by accelerating argon ions which were guided towards a metal target. The ion bombardment removed the atoms from the target material. The atoms fell down due to gravity and covered the fibre.

The coating used in submicrometre fibre metrology has to provide the following properties:

1. covering the whole surface and at the same time be as thin as possible.

2. Be very conductive, therefore it should not oxidate.

There are many materials available for coating but only gold and platinum confirmed the requirement. This materials have, however, a disadvantage. When the layer thickness is below 5 nm, they form clusters, so the surface is not completely covered by the coating (Fig. 3.4). Platinum clusters are smaller, which is better, but from financial reasons I used a gold target that was already available at CAESAR.

During sputtering, the atoms already could cluster while falling down from the material target to the sample. This effect could be weakened by setting the minimal distance between the specimen and the sputtering target (1 cm) [32]. Additionally, the lowest sputtering rate of 0.1 nm/s was chosen to decrease the density of the sputtered material in the buffer gas. The sputtering parameters for our machine were:

- Argon pressure: $5 \cdot 10^{-2}$ mbar

- Current: 30 mA

- Sputtering distance: 1 cm

Due to the small sputtering distance the fibre could be stripped from the substrate because of high electric fields close to the target. This was observed twice. Therefore gluing the fibre to the substrate was inevitable.

The coating layer thickness was measured by an built-in quartz scale [32] which gave the average thickness of the deposited material layer. For our sputtering machine, the manufacturer specified an accuracy of ± 1 nm for a 2 nm layer. After sputtering 2 nm of gold, the fibre stopped showing charging effects, although the surface was not covered completely due to clustering. An SEM image of an uncoated fibre is shown in Fig. C.1.

5. Imaging and image analysis

After determining the microscope settings and preparing the fibre, I performed the SEM imaging which was designed to improve the microscope accuracy and to avoid systematic errors.

The analysis of the SEM images was automatically done by a MATLAB program which I have written to speed up the process. In order to measure the fibre diameter, an image processing procedure was performed. Then the fibre diameter could be determined and recalibrated.

The obtained data was used to validate the optical fibre diameter measurement.

5.1. Imaging procedure

The imaging procedure was done with the microscope settings listed in Tab. 5.1.

Microscope setting	Value
Probe beam energy	20 keV
Specimen current	10 pA
Magnification	$\sim 500\,000$ times
Scan speed	300 ms/frame, 2.4 s/frame

Table 5.1.: SEM measurement setting for achieving the best resolution, avoiding fibre damage by probe beam and increasing detection efficiency (Sec. 3.3–3.5).

I have taken images along the fibre waist with a step of typically 0.5 mm. At each measurement position I have optimized the probe beam focussing and minimised the lens aberrations (Sec. 3.1). This could take a few minutes so the fibre could be narrowed during this time (Sec. 3.4). Therefore, this fibre section was not used for diameter measurement. That's why the scanning area was shifted by 2 µm (30 % of the maximal shifting distance) along the fibre and then the image was taken with a scan speed of 300 ms/frame. The same procedure was done to take the second image with a scan speed of 2.4 s/frame. I have written a macro that performed the imaging procedure automatically

(shifting the scanning area, taking the images) to minimise the exposure time of the fibre and thus prevent the narrowing. Additionally the fibre was positioned vertically in the image to reduce heating the fibre by the probe beam (Sec. 3.4).

A typical image is shown in Fig. 5.1 where the fibre does not cover the whole image. The distance between the fibre edge and the left and right image corners should be not less than $\sim 15\%$ of the image width. This was necessary done due to scanning speed change of the beam approaching the frame corner of and causing distorsion on the image.
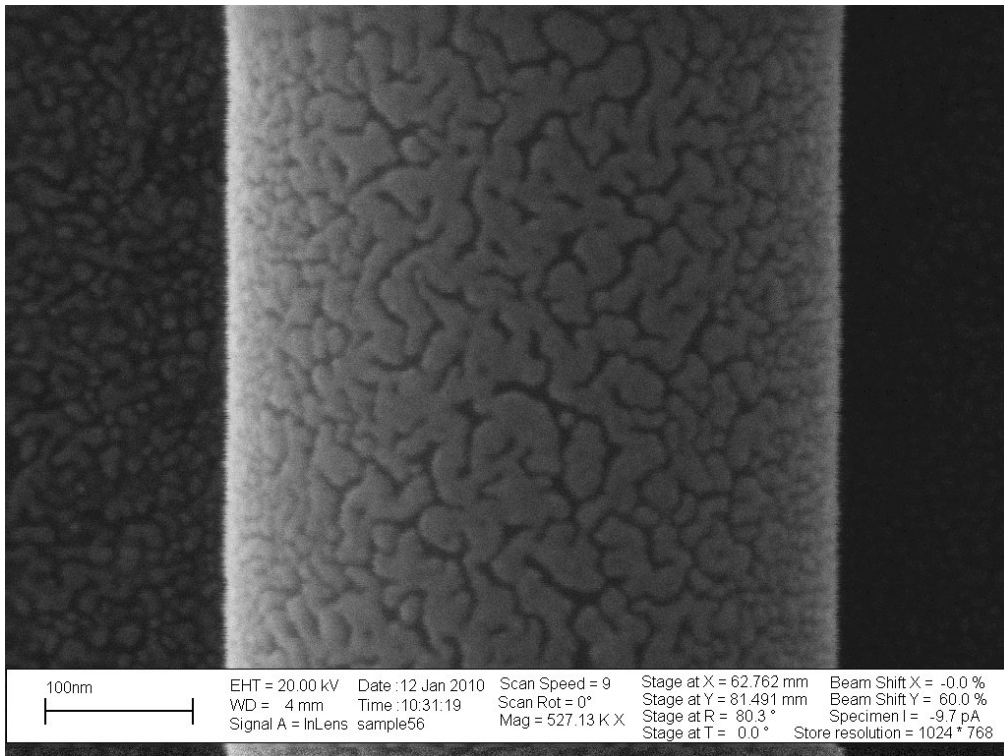
Figure 5.1.: A typical SEM image of the fibre waist. The structure on the fibre surface is due to gold coating which is approximately 2 nm thick.

5.2. Image processing

The MATLAB program performed the image processing automatically. The first step was to readout automatically the scale factor and the stage position (Fig. 5.2). This procedure is described in Sec. B. In the next step, the fibre zone was analysed. The upper 100 rows of the image were not used for analy-

Fibre zone

Figure 5.2.: Classification of zones on the SEM-images.

sis because of distortions resulting from the SEM controlling software and the irregularity in the speed of the scanning beam [21].

The image processing started with tilting the fibre to a vertical position. Although I paid attention to adjust the fibre in a vertical position, images taken with different scan speeds showed different tilting angles for the same fibre section. This was due to fluctuations of ma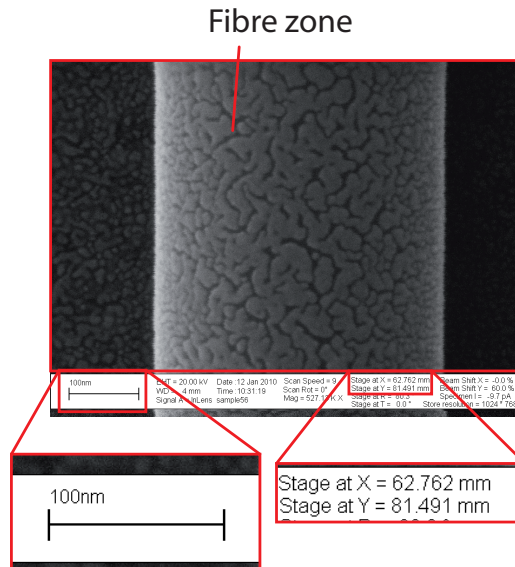gnetic and electric field inside the microscope chamber that slightly influenced the probe beam. This resulted in a shear of the image rows, therefore the tilting could be reverted by shifting each rows of the image.

The tilting angle was determined by comparing the centre of mass of the uppermost with the lowermost 50 rows. For that, vertical binning was applied to each group of rows separately, meaning that the sum of rows was taken and divided by the number of rows. From the resulting curves the centre of mass was taken to determine the tilting angle (Fig. 5.3a). From the angle, the shifting distance for each row was calculated. The rows were shifted by an integer number of pixels to obtain a vertical fibre position (Fig. 5.3b).

After the fibre tilt was corrected, vertical binning could be applied to the whole fibre zone. This procedure was necessary to reduce the noise of the image (Fig. 5.4). The diameter change within a imaged section could be neglected, since the waist represents a homogeneous part of the fibre (unlike the taper, where a slope of 3 mrad leaded to a diameter change of 6 nm within an image).

27
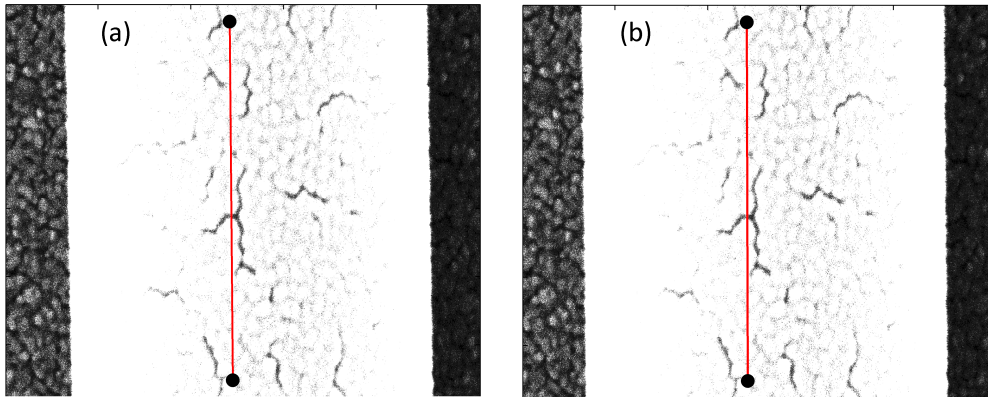
Figure 5.3.: Tilt correction of the fibre. The line indicates the fibre tilt. (a) Fibre is tilted at 0.5 º. (b) Fibre after tilt correction.

The last step of the image processing was the filtering of the binned profile. The requirements on the filter were the following: on the one hand the noise had to be reduced effectively, on the other hand the image contrast should be changed as little as possible. The moving average filter met the requirement [33]. It averaged a fixed number of neighbouring pixels and assigned the value to the first pixel in the group. This procedure was applied to all pixels in the binned curve.

Figure 5.4.: SEM image profiles. Upper curve: arbitrary row from an SEM image. Lower curve: fibre profile after image processing.

After the data processing the diameter of the fibre section could be determined.

5.3. Diameter determination

The fibre diameter could be determined from the image profile shown in Fig. 5.5a. The main task was to identify the fibre edge positions, located in the outer slopes of this curve. We used the edge detection model published by Rieger and van Veen [34]. This method relied on the fact that the 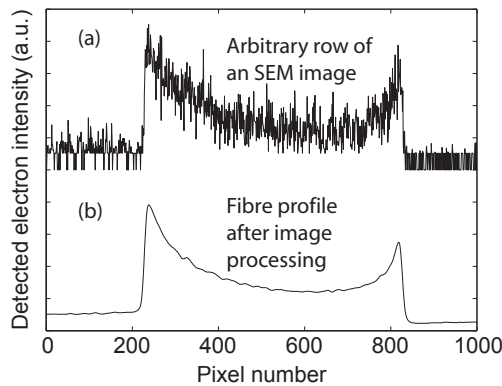edges could be approximately described by the error function $\mathrm{erf}(x)$, which is the integral of the Gaussian function:

$$\mathrm{erf}(x) = \frac{2}{\sqrt{\pi}} \int\limits_{0}^{x} \exp\left(\frac{t^2}{\sigma^2}\right) \mathrm{d}t \tag{5.1}$$

Therefore the derivative of the binned profile gave a Gaussian peak for the left slope and a dip for the right. Squaring the derivative resulted in two positive peaks a the positions of the fibre edges (Fig. 5.5b). The advantages of squaring the derivative are:

1. we obtain two positive peaks, which was easier to handle in the MATLAB program

2. it enhances the peak height for a more reliable peak detection.

Each peak was fitted by the Gaussian function to obtain the peak position and the Gaussian σ. The peak position corresponded to the maximal contrast change
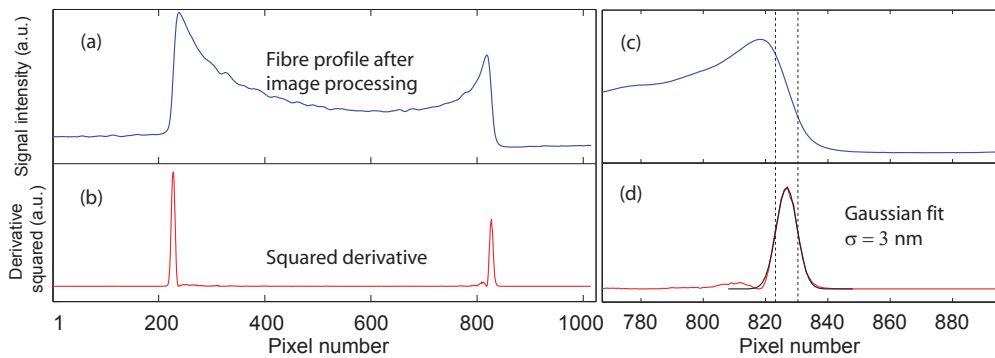
Figure 5.5.: Edge detection from the fibre profile. (a) Fibre profile obtained by image processing. (b) Squared derivative of the fibre profile. (c) Right edge of the fibre profile. (d) Squared derivative of the right edge. Peak position determines the edge position. Dashed lines illustrate the $\pm\sigma$ error.

in the image which was assumed to be the edge of the fibre. The Gaussian σ gave the information of the slope steepness and thus the uncertainty of the diameter

determination [34]. Therefore the program took $\pm\sigma$ as the error of the edge determination (Fig. 5.5c,d). So the diameter was the distance between the fibre edges and the diameter error was the sum of the σ's obtained from the fitting of both edges. This method provided a systematic uncertainty due to not taking into account the cylindrical fibre shape.

A more exact edge determination would have required the simulation of the electron-fibre interaction and the emission of the secondary electrons. To our knowledge, a model taking into account the cylindrical shape of the fibre did not exist. A short introduction of edge detection for sharp edges is given in Sec. A and a detailed in-sight is provided by Villarrubia in [35, 36, 37].

The obtained diameter in pixel was converted to micrometer using the scale factor. In this way I could automatically analyse a set of images taken along the fibre. An example of such a measurement is given in Fig. 5.6. Each data
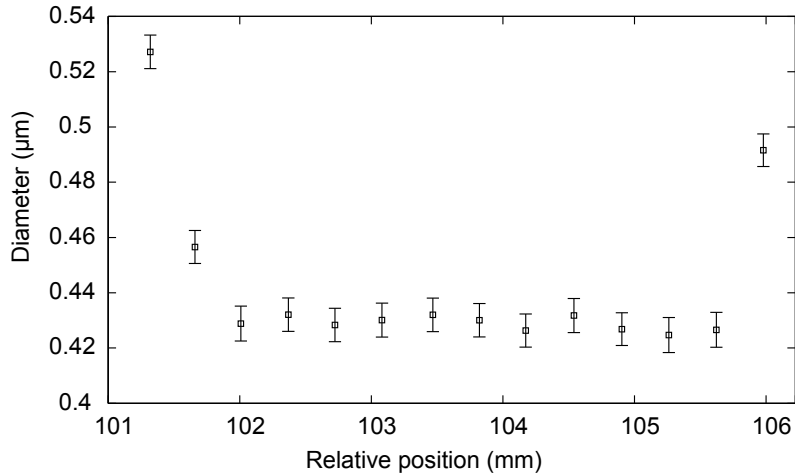
Figure 5.6.: Diameter measurement along the fibre.

point corresponds to the diameter obtained from an SEM image. The distance between two data points is 0.5 mm, so both the tapers and the waist can be resolved. Although the systematic uncertainty in edge detection is high, the relative error is low, which allows us to compare the diameters obtained from different images. Therefore the plot in Fig. 5.6 gives a realistic view of the diameter inhomogeneity in the waist.

5.4. Calibration

The certified accuracy of the SUPRA 55 was 10 % for all sets of measurement settings (i.e. probe beam energy, scanning speed, magnification etcetera). The initial calibration was done by Zeiss for a particular set of propperties. For this set the accuracy was better than 10 % but a change of even one parameter worsened it by an unknown factor. Therefore, to obtain the best accuracy recalibration was required.

Figure 5.7.: Calibration target Plano S1995A (left part). On the right: two SEM images of the calibration patterns (10 µm and 0.5 µm period)

I have done the recalibration of the microscope using a calibration target (Plano S1995A) that provided 5 calibration regions with parallel lines of known periods (0.5, 1, 2, 5, and 10 µm). Fig. 5.7 illustrates the calibration target. On the right side, the figure shows SEM images of two calibration patterns. In order to obtain the recalibration factor, I imaged the calibration patterns for each set of measurement settings and determined the line distance. The image analysis was done with the MATLAB program.
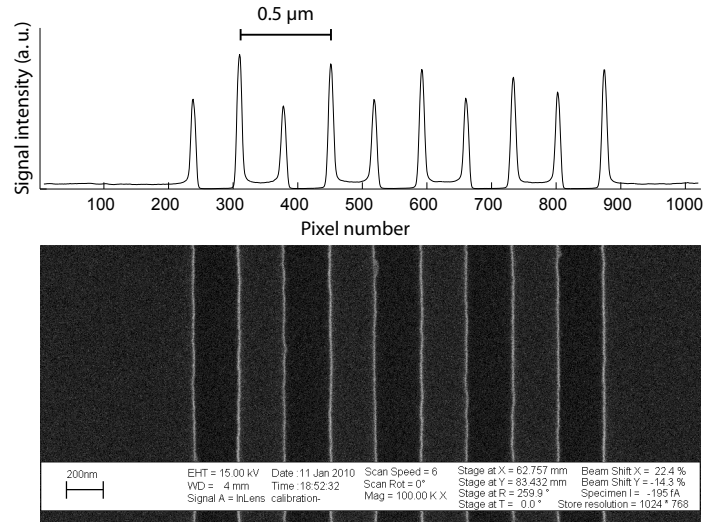
First step was to apply vertical binning and taking the positions of the maxima of the binned curve. The recalibration factor was then determined by calculating the ratio between the known line distance and the measured line distance. This procedure was done for all calibration patterns and the average of the obtained recalibration factors was taken. The average factor was then used to recalibrate the diameter values. A recalibrated measurement, compared to a not recalibrated, is shown in Fig. C.3.

The specified accuracy of the calibration patterns were between ±0.19 % (10 µm period pattern) and ±0.78 % (0.5 µm period pattern). However, the error is due to the accuracy of the manufacturing process. The calibration target was not certified by the PTB (Physikalisch-Technische Bundesanstalt).

We have chosen the conservative approach of taking the highest error. For a typical fibre diameter (500 nm) this gives an error of ±4 nm.

Figure 5.8.: SEM image of the calibration target S1995A.

5.5. Verification by the SEM measurement

After the SEM images were analysed and calibrated, they could be compared to the diameter values obtained with our harmonic-generation technique. An example of such a waist diameter measurement is shown in Fig. 5.9a. The
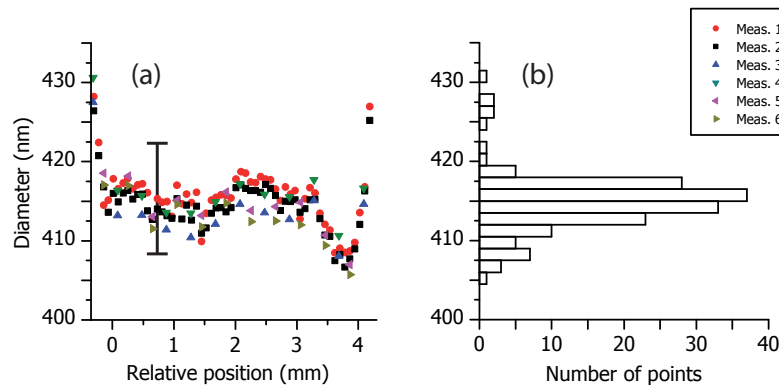

Figure 5.9.: (a) Waist diameter profile obtained by SEM measurements of different beam energies and scan speeds. Each data point was measured with an accuracy of ±7 nm, indicated by the error bar for one data point. (c) Diameter histogram.

illustrated measurements 1–6 differ by the probe energy and scan speed. Mea-

surements 3 and 5 (4 and 6) were imaged with the same settings but with a time delay of several hours. Each diameter value was measured with an accuracy of ± 7 nm. The origins of the almost pure systematic error are listed in Tab. 5.2. However, the precision of the SEM measurement is better than ± 4 nm, which allows to resolve the thinner part on the right side of Fig. 5.9a.

Source	Value	Comment
Edge determination on SEM image	± 6 nm	Systematic uncertainty of the image analysis method (Sec. 5.3)
SEM recalibration	± 4 nm	Error of the calibration target (Sec. 5.4)
Gold coating thickness variation	± 2 nm	According to manufacturer (Bal-Tec) (Sec. 4.2)
Total:	± 7 nm	

Table 5.2.: SEM error contributions

To compare both measurement methods I extract the value of the dominating diameter from the SEM measurement by taking the histogram of the diameter values (Fig. 5.9b). The main peak represents the dominating diameter of the tapered optical fibre. Since the accuracy of each diameter is 7 nm and the bin size is 1.5 nm, the accuracy of the peak position is $(\pm 7 \text{ nm}) + (\pm 0.75 \text{ nm}) \approx \pm 7$ nm.

The dominating value can be compared to the optically obtained diameter. Fig. 5.10 shows a plot of optically obtained fibre waist diameter (d_{optical}) versus diameter obtained by SEM (d_{SEM}). The dashed line gives the ideal case of coincidence. The origin of the errors of d_{optical} is described in [17]. The plot shows an offset ($d_{\text{optical}} < d_{\text{SEM}}$), which results from an unknown systematic error. Since the theory of phase matching in tapered optical fibres is well known, I assume the shift being due to the SEM technique. The most probable origin is the edge detection method which does not take into account the cylindrical shape of the fibre (Sec. 5.3). An other origin might be due to the calibration target, since it is not certified.

However, the histogram and the second-harmonic response in Fig. 2.3 show similar structures:

1. the tail at higher diameters due to the taper

2. the main peak due to the dominating diameter

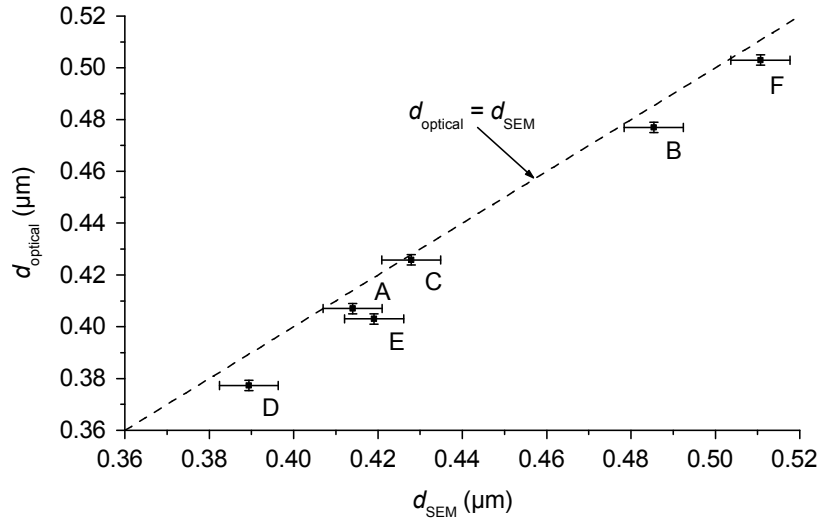3. the minor peak at low diameter due to thinner waist part

Figure 5.10.: The fibre diameter measured by harmonic generation (d_{optical}) vs. the diameter as measured by SEM (d_{SEM}) for samples A to F.

4. the cut-off due to the absence of smaller diameters.

Despite the shift in Fig. 5.10, the SEM measurement proves that the optical signal can be interpreted as an effective diameter measurement.

6. Conclusion

In this thesis I have presented a method to measure submicrometre diameter of tapered optical fibres. It includes the preparation of fibres for electron beam exposure and the imaging procedure that minimize systematic errors. Furthermore I have written a MATLAB program that automatically analyses the SEM images. Using this method I verified the non destructive, optical diameter measurement technique, which was developed in our group.

In future, the SEM method could be improved in several steps. On the one hand, a certified calibration target with a period of less than 500 nm could be used. On the other hand, an exact edge detection model could be developed that takes into account the cylindrical shape of the fibre. This could be done by simulating the electron-specimen interaction for a scanning beam and for different fibre diameters. The simulated signals could be fitted to the measured data to find out the fibre diameter.

Additionally the scale of the sputtering machine could be calibrated by depositing a thin gold layer (2 nm) on a thin membrane. The thickness of the gold layer could be measured with a calibrated TEM. In this way, the cluster structure and the coating thickness could be analysed.

A different approach of improving the verification of the optical method would be a cross check of the fibre diameter with a TEM. This measurement would require a different way of fibre preparation. The fibre waist should be placed on a TEM grid with a period of ~ 10 nm to prevent the fibre from vibrating. After that the whole sample should be coated by the evaporating technique which allows to cover the specimen from all sides. Such a fibre could be measured with TEM as well as with SEM to compare the techniques with the optical measurement.

A. Surface effects

As explained in section 3.2, the detected SE signal is generated in the 5λ region close to the specimen surface. Scanning over a slope increases the impact area of the probe beam and consequently the escape region of the secondary electrons, which is illustrated in figure A.1a. This leads to a higher SE signal intensity
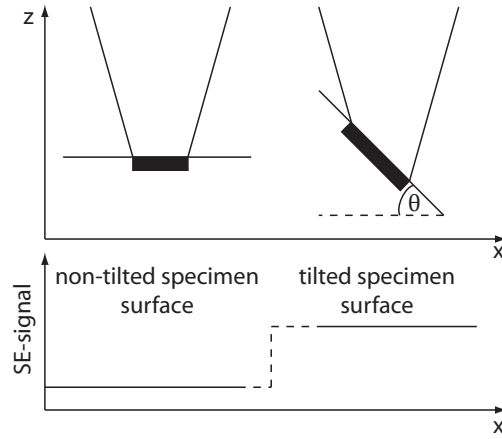

Figure A.1.: Upper part: Escape volume of the secondary electrons (SE). The volume increases on the slope of the surface. Lower part: the SE-signal intensity increases scanning from a non-tilted to a tilted specimen surface.

generated in the slope region. Figure A.1b compares the detected SE signal intensities for a non-tilted and a tilted specimen surface. As the angle of the tilt increases, the SE intensity increases. Therefore the SE signal intensity is a function of the tilting angle θ [38]

$$I_{\mathrm{SE}} = \propto \sec(\theta) \tag{A.1}$$

Due to the cylindrical fibre shape the transversal profile can be described by the secant function. However, close to the fibre edge the secant approximation fails because of the singularity at $\theta = \pm 90\ ^\circ$.

At the edge an additional effect interferes. When the probe beam and thus the interaction volume reaches the edge, the effective SE response area increases which leads to a higher SE signal intensity. The simplest case, a sharp edge, is illustrated in figure A.2a. On the left side the beam causes a SE-response

in the upper direction. Going further towards the edge (right beam position) the interaction volume additionally releases secondary electrons at the edge. Therefore, at the position of the sharp edge, the SE signal intensity is doubled [21]. The increase of the intensity at the sharp edge can be described by an
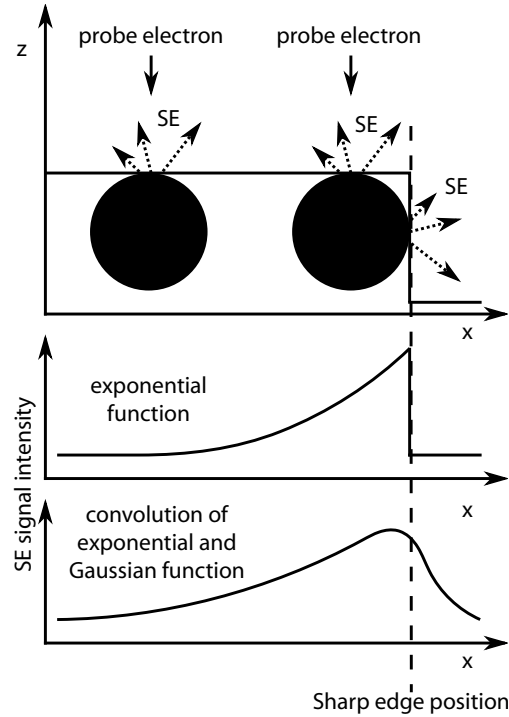

Figure A.2.: Specimen response, model

exponential function shown in figure A.2b. The maximum of the response signal intensity is located at the position of the edge. The convolution of this curve with the Gaussian distribution, due to probe beam shape, gives the measured signal sketched in figure A.2c. Nevertheless, the round edge of the fibre can not be described by the pure exponential function because of the interference of tilt and the edge effects.

B. Image processing

B.1. Scale bar

First the length of the scale bar in pixels is determined. The scale bar line is two pixels thick, so two pixels have to be subtracted from the estimated value. Then the readout of the number that gives the length of the scale bar in metric units follows. The possible entries are: 10 nm, 20 nm, 30 nm, 100 nm, 200 nm, 1 µm, and 1 µm. Reference images for each value were saved to the MATLAB program before. The reference images are compared with the entry by subtraction of the readout array from each reference array. If the array coincide, the subtraction result is zero. When the number n_{scale} is identified, the scale factor f_{scale} can be calculated by

$$f_{\mathrm{scale}} = \frac{n_{\mathrm{scale}}}{p_{\mathrm{scale}}} \tag{B.1}$$

where p_{scale} is the scale bar length in pixel. Therefore a distance on the SEM-image (in pixel) can be calculated by multiplying it with f_{scale}.

B.2. Stage position

The stage position readout works in the same way. The program reads out the numbers one by one, compares them to the reference image and determines the value. The method of comparing the reference image with the entry in the data zone by subtraction is very stable to errors. When the entry and the reference image perfectly coincide, the method gives a zero, which assures that the number was identified. A number not equal to zero indicates an error, so the program stops in order not to give a wrong number.
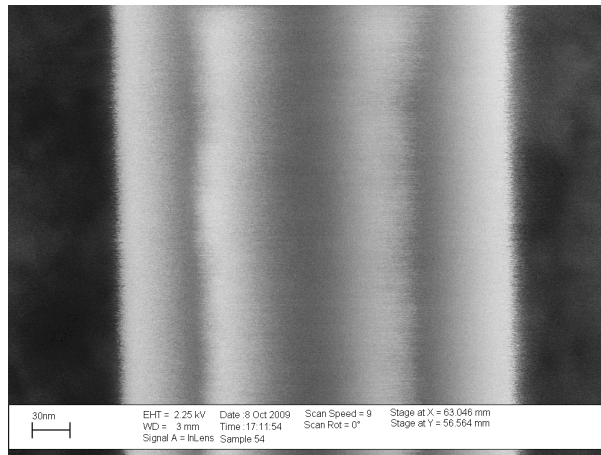
C. Figures

Figure C.1.: SEM-image of an uncoated fibre. The bright and dark regions on the fibre surface indicate charged regions.
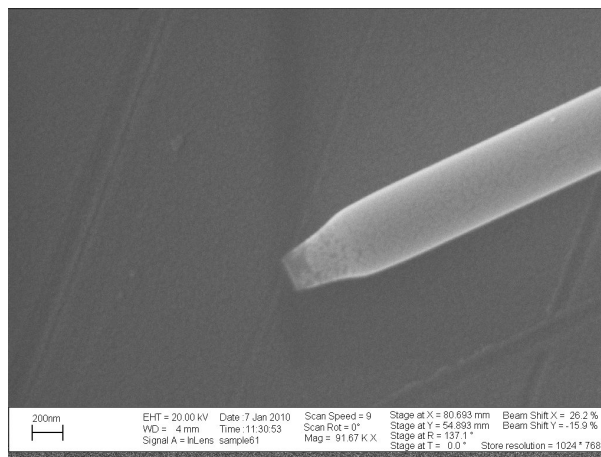

Figure C.2.: Broken fibre after a view seconds of scanning. First the fibre got thinner (see also Fig. 3.4). Than suddenly is broke and flew apart. The broken end was found 1 mm away from its original position.
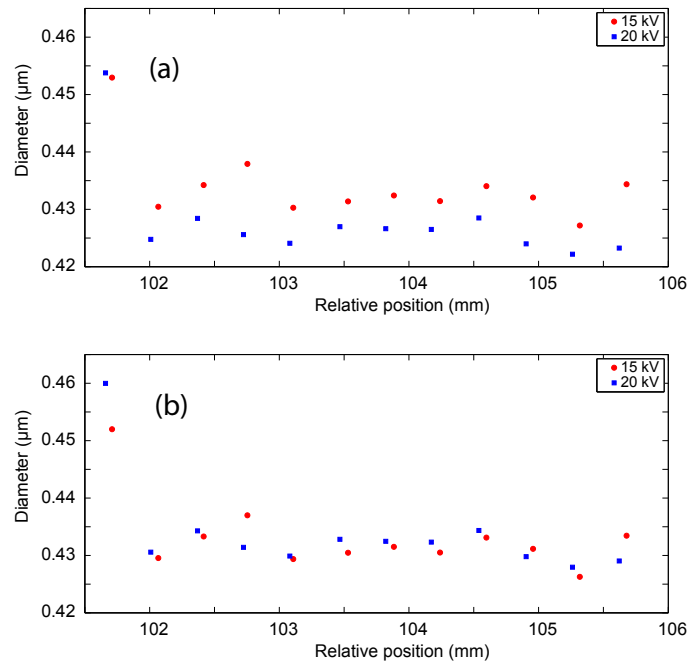
Figure C.3.: Two diameter measurement with identical microscope settings except the probe energy. (a) Not calibrated. (b) Calibrated. Note, that the sets images were made at different positions on the fibre. The distance between two data points of different sets is typically 100 µm. Therefore the obtained diameter values can slightly differ due to inhomogeneity of the fibre waist.

Bibliography

[1] H. Stintzing. Method and device for automatically assessing, measuring and counting particles of any type, shape and size., 1929.

[2] M. Knoll and E. Ruska. Das elektronenmikroskop. *Z. Phys.*, 78:318–339, 1932.

[3] Mark A. Foster, Amy C. Turner, Michal Lipson, and Alexander L. Gaeta. Nonlinear optics in photonic nanowires. *Opt. Express*, 16(2):1300–1320, 2008.

[4] Gilberto Brambilla, Fei Xu, Peter Horak, Yongmin Jung, Fumihito Koizumi, Neil P. Sessions, Elena Koukharenko, Xian Feng, Ganapathy S. Murugan, James S. Wilkinson, and David J. Richardson. Optical fiber nanowires and microwires: fabrication and applications. *Adv. Opt. Photon.*, 1(1):107–161, 2009.

[5] Jonathan M. Ward, Danny G. O'Shea, Brian J. Shortt, Michael J. Morrissey, Kieran Deasy, and Síle G. Nic Chormaic. Heat-and-pull rig for fiber taper fabrication. *Review of Scientific Instruments*, 77(8):083105, 2006.

[6] Florian Warken, Arno Rauschenbeutel, and Thomas Bartholomäus. Fiber pulling profits from precise positioning. *Photonics Spectra*, 42(3):73, March 2008.

[7] Rafael R. Gattass, Geoffry T. Svacha, Limin Tong, and Eric Mazur. Supercontinuum generation in submicrometer diameter silica fibers. *Opt. Express*, 14(20):9408–9414, 2006.

[8] G. Sagué, E. Vetsch, W. Alt, D. Meschede, and A. Rauschenbeutel. Cold-atom physics using ultrathin optical fibers: Light-induced dipole forces and surface interactions. *Phys. Rev. Lett.*, 99(16):163602, Oct 2007.

[9] Florian Warken, Eugen Vetsch, Dieter Meschede, Moriz Sokolowski, and Arno Rauschenbeutel. Ultra-sensitive surface absorption spectroscopy using sub-wavelength diameter optical fibers. *Opt. Express*, 15(19):11952–11958, 2007.

[10] S. M. Spillane, G. S. Pati, K. Salit, M. Hall, P. Kumar, R. G. Beausoleil, and M. S. Shahriar. Observation of nonlinear optical interactions of ultralow levels of light in a tapered optical nanofiber embedded in a hot rubidium vapor. *Phys. Rev. Lett.*, 100(23):233602, Jun 2008.

[11] Florian Warken and Harald Giessen. Fast profile measurement of micrometer-sized tapered fibers with betterthan 50-nm accuracy. *Opt. Lett.*, 29(15):1727–1729, 2004.

[12] M. Sumetsky, Y. Dulashko, J. M. Fini, A. Hale, and J. W. Nicholson. Probing optical microfiber nonuniformities at nanoscale. *Opt. Lett.*, 31(16):2393–2395, 2006.

[13] U. Österberg and W. Margulis. Dye laser pumped by nd:yag laser pulses frequency doubled in a glass optical fiber. *Opt. Lett.*, 11(8):516–518, 1986.

[14] Ulf Österberg and Walter Margulis. Experimental studies on efficient frequency doubling in glass optical fibers. *Opt. Lett.*, 12(1):57–59, 1987.

[15] E M Dianov and D S Starodubov. Photoinduced generation of the second harmonic in centrosymmetric media. *Quantum Electronics*, 25(5):395–407, 1995.

[16] P. G. Kazansky and P. St. J. Russel. Thermally poled glass: frozen-in electric field or oriented dipoles? *Opt. Commun.*, 110(5–6):611–614, 1994.

[17] Ulrich Wiedemann, Konstantin Karapetyan, Cristian Dan, Dimitri Pritzkau, Wolfgang Alt, Stephan Irsen, and Dieter Meschede. Measurement of submicrometre diameters of tapered optical fibres using harmonic generation. (To be published in Opt. Express).

[18] Allan Snyder and John Love. *Optical waveguide theory*. Chapman & Hall, London, 1983.

[19] Limin Tong, Jingyi Lou, and Eric Mazur. Single-mode guiding properties of subwavelength-diameter silica and silicon wire waveguides. *Opt. Express*, 12(6):1025–1035, 2004.

[20] A. V. Crewe, D. N. Eggenberger, and J. Wall. Electron gun using a field emission source. *Rev. Sci. Instrum.*, 39:576–583, 1968.

[21] Joseph Goldstein, Dale E. Newbury, David C. Joy, Charles E. Lyman, Patrick Echlin, L.C. Lifshin, Ericand Sawyer, and J.R. Michael. *Scanning electron microscopy and x-ray microanalysis*. Springer, 3rd edition, 2003.

[22] T. E. Everhart and R. F. M. Thornley. Wide-band detector for micro-microampere low-energy electron currents. *Journal of scientific instruments*, 37:247 – 248, 1960.

[23] *Zeiss SUPRA 55 operator manual*.

[24] Kenji Murata, Takayuki Matsukawa, and Ryuichi Shimizu. Monte carlo calculations on electron scattering in a solid target. *Jpn. J. Appl. Phys.*, 10:678–686, 1971.

[25] D. F. Kyser and K. Murata. Quantitative electron microprobe analysis of thin films on substrates. *IBM J. Res. Dev*, 18:352–363, 1974.

[26] H. Seiler. Secondary electron emission in the scanning electron microscope. *J. Appl. Phys.*, 54:R1, 1983.

[27] T. Koshikawa and R. Shimizu. A monte carlo calculation of low-energy secondary electron emission from metals. *J. Phys. D Appl. Phys.*, 7:1303–1315, 1974.

[28] Niedrig H. *Scanning*, 1:17, 1978.

[29] H. Seiler. *Z. Angw. Phys.*, 22:249, 1967.

[30] Dominique Drouin, Alexandre RÃľal Couture, Dany Joly, Xavier Tastet, Vincent Aimez, and Raynald Gauvin. Casino v2.42 - a fast and easy-to-use modeling tool for scanning electron microscopy and microanalysis users. *Scanning*, 29:92–101, 2007.

[31] David B. Williams and C. Barry Carter. *Transmission Electron Microscopy: A Textbook for Materials Science*. Springer, 2009.

[32] Patrick Echlin. *Handbook of sample preparation for scanning electron microscopy and x-ray microanalysis*. Springer, 2009.

[33] Alan Conrad Bovik. *Handbook of image and video processing*. Academic Press, 2005.

[34] B. Rieger and G. N. A van Veen. Method to determine image sharpness and resolution in scanning electron microscopy images. In M. Luysberg, K. Tillmann, and T. Weirich, editors, *EMC 2008 14th European Microscopy Congress, Vol. 1: Instrumentation and Methods*, pages 613–614, Heidelberg, 2008. Springer.

[35] J. S. Villarrubia, A. E. Vladar, J. R. Lowney, and M. T. Postek. Scanning electron microscope analog of scatterometry. *Proceedings of SPIE, Metrology, Inspection, and Process Control for Microlithography XVI, Daniel J. C. Herr, Editor*, 4689:304–312, 2002.

[36] J. S. Villarrubia, A. E. Vladar, and M. T. Postek. A simulation study of repeatability and bias in the cd-sem. *Journal of Microlithography Microfabrication and Microsystems*, 4(3):1–10, July 2005.

[37] John S. Villarrubia and Zejun J. Ding. Sensitivity of scanning electron microscope width measurements to model assumptions. *J. Micro/Nanolith. MEMS MOEMS*, Vol. 8:033003, 2009.

[38] H. Kanter. Energy dissipation and secondary electron emission in solids. *Phys. Rev.*, 121(3):677–681, Feb 1961.

Ich versichere, dass ich diese Arbeit selbstständig verfasst und keine anderen als die angegebenen Quellen und Hilfsmittel benutzt sowie Zitate kenntlich gemacht habe.

Referent: Prof. Dr. Dieter Meschede
Koreferent: Prof. Dr. Martin Weitz